

Review

Phase-Matching in Nonlinear Crystal-Based Monochromatic Terahertz-Wave Generation

Pengxiang Liu ^{1,2}, Chuncao Niu ^{1,2}, Feng Qi ^{2,3,4,*}, Wei Li ^{1,2}, Weifan Li ^{2,3,4}, Qiaoqiao Fu ^{2,3,4}, Liyuan Guo ^{2,3,4} and Zhongyang Li ⁵

¹ College of Information Engineering, Shenyang University of Chemical Technology, Shenyang 110142, China

² Shenyang Institute of Automation, Chinese Academy of Sciences, Shenyang 110169, China

³ Key Laboratory of Liaoning Province in Terahertz Imaging and Sensing, Shenyang 110169, China

⁴ Key Laboratory of Opto-Electronic Information Processing, Chinese Academy of Sciences, Shenyang 110169, China

⁵ College of Electric Power, North China University of Water Resources and Electric Power, Zhengzhou 450045, China

* Correspondence: qifeng@sia.cn

Abstract: Optically pumped nonlinear frequency down conversion is a proven approach for monochromatic terahertz (THz)-wave generation that provides superior properties such as continuous and wide tunability as well as laser-like linewidth and beam quality. Phase-matching (PM) is an important connection between the pump sources and nonlinear crystals and determines the direction of energy flow (as well as the output power). In past decades, a variety of peculiar PM configurations in the THz region have been invented and are different from the traditional ones in the optical region. We summarize the configurations that have been applied in nonlinear THz-wave generation, which mainly fall in two categories: scalar (collinear) PM and vector PM (including macroscopic noncollinear PM and microscopic vector PM). The development of this technique could relax the matching conditions in a wide range of nonlinear crystals and pump wavelengths and could finally promote the improvement of coherent THz sources.

Keywords: coherent terahertz source; nonlinear optics; phase-matching; nonlinear optical crystal; optical frequency conversion



Citation: Liu, P.; Niu, C.; Qi, F.; Li, W.; Li, W.; Fu, Q.; Guo, L.; Li, Z. Phase-Matching in Nonlinear Crystal-Based Monochromatic Terahertz-Wave Generation. *Crystals* **2022**, *12*, 1231. <https://doi.org/10.3390/cryst12091231>

Academic Editor: Martin Dressel

Received: 8 August 2022

Accepted: 24 August 2022

Published: 1 September 2022

Publisher's Note: MDPI stays neutral with regard to jurisdictional claims in published maps and institutional affiliations.



Copyright: © 2022 by the authors. Licensee MDPI, Basel, Switzerland. This article is an open access article distributed under the terms and conditions of the Creative Commons Attribution (CC BY) license (<https://creativecommons.org/licenses/by/4.0/>).

1. Introduction

Terahertz (THz) technology [1] has attracted considerable interest owing to the unique properties of this band of electromagnetic waves: (1) resonance with vibrational and rotational modes of typical large molecules, (2) spectral overlap with the background radiation of the space, (3) penetration through general non-polar materials (e.g., packages), and (4) low photon energy (unionized to biological tissues). A variety of applications in analytical chemistry [2], astronomy [3], the quality control of industrial products [4], biomedical imaging and diagnose [5], etc., have demonstrated the effectiveness of this technology. As active spectral analysis systems, Fourier transform infrared (FTIR) and time-domain spectroscopy (TDS) are well-established and often utilized. Those methods based on widely tunable and monochromatic THz sources (i.e., frequency-domain spectroscopy) are alternative tools to FTIR and TDS due to their high spectral resolution.

Nonlinear optical frequency down conversion from the laser to the THz wavelength, commonly referred to as difference frequency generation (DFG) or stimulated polariton scattering (SPS), is one of the most effective approaches and could provide the following merits: the availability of a compact pump laser and nonlinear crystals, operation at room temperature, continuous and wide tunability, and laser-like linewidth and beam quality. As discussed by C.M. Armstrong [6], “for some applications, the source’s spectral purity, tunability, or bandwidth is more important”. These kinds of coherent sources have been

successfully applied in various fields for applications such as the identification of gas species [7], quality evaluations of pharmaceuticals [8], and nondestructive inspection via spectroscopic imaging [9].

In the past few decades, a number of efforts have been made to improve the performance of optical THz sources: from pump lasers via nonlinear crystals to enhancement configurations (including surface-emitted [10], external cavity [11], and waveguide [12] configurations, among others). In the down conversion process, the lasers and THz-waves are mainly coupled through nonlinear susceptibility $\chi^{(2)}$, so phase-matching (PM) is a key factor. It determines the output characteristics of the THz source according to these aspects: (1) the direction of energy flow during the three-wave interaction, (2) the available effective nonlinear coefficient d_{eff} , (3) the suitable pump wavelength (if the laser is powerful), (4) the matchable tuning range, and (5) the tolerance of the angle, wavelength, or temperature (if precise control is necessary). Numerous PM geometries have been adopted according to the optical properties of nonlinear crystals. Some of them (e.g., birefringent, noncollinear, and quasi-PM) are extended from traditional optical regions; some, were original developments (such Cherenkov-type and front-tilting PM [13,14]).

We classify these geometries into two main categories: scalar and vector PMs. In the case of scalar PM, the three beams are collinear (forward or backward output coupling [15,16]). In the other category, a wavevector triangle is properly designed, and the THz output is commonly coupled in a lateral direction. The vector PMs are further divided into two types: macroscopic noncollinear PM (quasi-plane waves in obviously different directions [17]) and microscopic vector PM (between spatial Fourier components [18,19]).

This paper is organized as follows. First, we introduce the basic problem of PM in THz-wave generation and compare it to that in the optical region in Section 2. A brief review of PM geometries obtained via various methods is presented in Sections 3 and 4. The mechanisms of each method is described, and the suitable nonlinear crystals and typical reports are presented. Here, we mainly discuss the interaction between two monochromatic optical waves rather than the optical rectification of ultra-short pulses. Section 3 concerns the scalar (collinear) forms, including birefringent PM in traditional infrared crystals (GaSe/ZnGeP₂), the cross-reststrahlen band PM in zinc blende or organic crystals, and quasi-PM (QPM) in ferroelectrics or zinc blende crystals. The vector forms are considered in Section 4, which consists of two Sections 4.1 and 4.2, for the macroscopic noncollinear and microscopic vector PMs, respectively. In Section 4.2, Cherenkov-type, surface-emitted QPM and modal PM are considered. Moreover, other configurations are also enumerated. A summary of the current progress and perspectives is given in Section 5.

2. Basic Problem of Phase-Matching in THz-Wave Generation

The down conversion process is, in essence, energy flow from a high-frequency optical wave (called a “pump”) to a low-frequency optical wave (called a “seed” or “Stokes”) and a THz-wave via non-resonant $\chi^{(2)}$ coupling [20]. The delivered THz frequency depends on the seed wavelength or cavity feedback, which obeys the energy conservation relationship. The configurations of dual-wavelength input are referred to as DFG or injection-seeded THz parametric generation (is-TPG). If the intensities of the two beams are comparable, it is called DFG, and if one is much stronger than the other, it is called is-TPG. In the case of single-wavelength input, a cavity is usually necessary. This process is initially called THz parametric oscillation (TPO) and has recently been called SPS. Although TPO/SPS is considered to be a mixing of second-order parametric processes and third-order Raman scattering in some literature [17], energy conservation and PM still dominate.

The concept of PM has been explained from three points of view: (1) a constructive interference between the fields driven by polarization at different propagation steps [21], (2) momentum (wave vector) conservation, and (3) phase-dependent energy flow from polarization to the field based on Poynting’s theorem [22]. Mathematically, the PM condition is expressed as

$$\vec{\Delta k} = \vec{k}_p - \vec{k}_s - \vec{k}_T = \vec{0} \quad (1)$$

where the subscripts p, s, and T denote the pump, seed/Stokes, and THz-waves, with $\omega_p = \omega_s + \omega_T$ and $\omega_p > \omega_s \gg \omega_T$. In a scalar (forward collinear) form, (1) is equivalent to

$$n_p \omega_p - n_s \omega_s - n_T \omega_T = (n_p - n_s) \omega_s + (n_p - n_T) \omega_T = 0 \tag{2}$$

Then, the problem of PM turns into a problem of refractive index matching, which is greatly influenced by the dispersion property of nonlinear crystals.

For a comparison with the traditional optical region (all three waves in one normal dispersion region), we introduce the subscripts 3, 2, and 1 to denote three optical waves, with $\omega_3 = \omega_2 + \omega_1$, $\omega_3 > \omega_2 \geq \omega_1$, and $n_3 > n_2 \geq n_1$. As a result, the collinear wave vector mismatch Δk_{opt} is always positive, and a vector triangle will not help to make it zero if all of the refractive indices are on one dispersion curve (isotropic medium or the same polarization).

The wavevector mismatch can be expanded as another form:

$$\Delta k = k_p - k_s - k_T = \frac{\partial k}{\partial \omega} (\omega_p - \omega_s) - \frac{n_T}{c} \omega_T = \frac{\omega_T}{c} (n_g - n_T) \tag{3}$$

where $n_g = c(\partial k / \partial \omega)$ is the optical group index.

The PM in the THz region differs from that in the optical region in two main ways. First, the THz and pump frequencies lie across one or more absorption bands (the reststrahlen band), which breaks the strict relationship above: $\Delta k_{opt} > 0$. On the contrary, the THz refractive index is commonly equal to or larger than the optical one (i.e., $\Delta k_{THz} \leq 0$). Collinear PM in isotropic crystals [23] and type-0 (eee-type) PM [24] are possible. The corresponding medium ($n_T \approx n_g$) is called “subluminal” or “weakly superluminal” material [25]. In the general case of $\Delta k_{THz} < 0$, noncollinear geometry [17] could work, even in strong superluminal materials (n_T much larger, e.g., ferroelectric). Second, the THz wavevector is much smaller, and its transverse Fourier component is more prominent. Thus, some configurations such as backward [16] and Cherenkov-type THz emissions [13] can be achieved, which are rarely observed in the optical region. The choice of PM geometry is further enriched, and some of the strict PM conditions are relaxed. In the following sections, different types of PMs are summarized and classified, as seen in Figure 1.

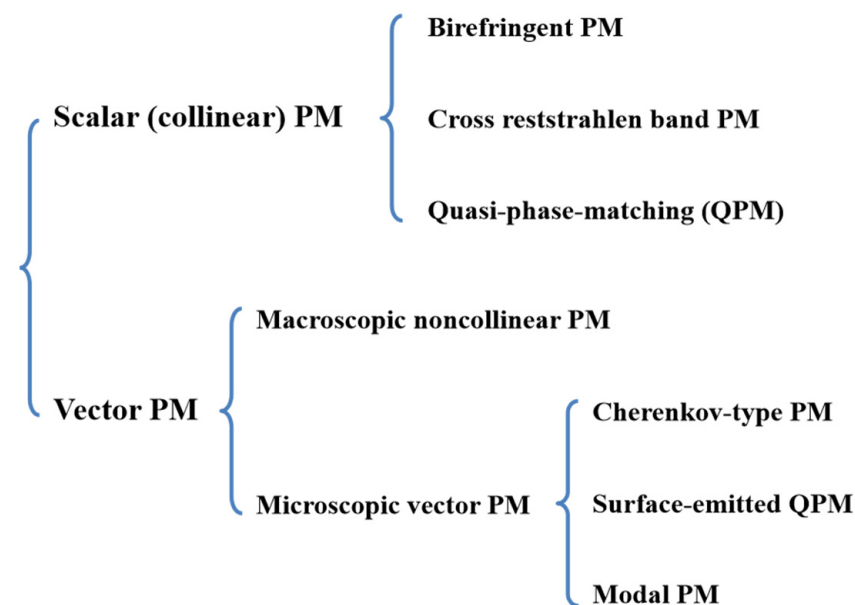


Figure 1. Classification of phase-matching in nonlinear THz-wave generation.

3. Scalar (Collinear) Phase-Matching

A collinear interaction is favorable due to the overlapping area of the large beams and the ease of alignment. The inherent difference between the refractive indices can be com-

compensated for by the birefringence or cross-reststrahlen band in bulk crystals or by artificial periodic poling/inversion structures. In major situations [15,23,24,26], THz outputs are in the same direction as the input beams (forward coupling); in minor situations [16,27], outputs are in the opposite direction (backward coupling).

Birefringent Phase-Matching

Birefringent PM has been widely adopted in nonlinear processes in optical regions. One of its merits is its broadband and frequency-agile tunability that can be achieved by rotating the crystal. In some traditional non-oxide infrared crystals (such as GaSe [15,16,28–34] and ZnGeP₂ [35–38]), birefringent PMs are extended to THz DFG.

In the past 20 years, GaSe (negative uniaxial) crystals have attracted a large amount of attention in nonlinear THz-wave generation due to their extremely low THz absorption and collinear PM. Two forward configurations have been investigated for different frequency band generation techniques [28]. In the scheme for low-frequency bands (Figure 2a), the input pump (1.06 μm) and seed (1.06–1.09 μm) lights are ordinary (slow) and extraordinary (fast), delivering a fast THz-wave (0.0848–5.15 THz). The band is labeled as o-e \rightarrow e or oee-type, with an effective nonlinear coefficient of $d_{22}\cos^2\theta\cos 3\varphi$ and an optimal φ of 0° . In fact, the element d_{16} works in the nonlinear coupling and is equal to $-d_{22}$ according to the crystal symmetry. The scheme for the high-frequency bands (also regarded as mid-infrared) is shown in Figure 2b, and the bands are labeled as eoo-type. A tuning range of 7.81–111 THz (38.4 to 2.7 μm) can be obtained by rotating the crystal in the range from 35° to 75° . Backward THz-wave DFG has also been demonstrated with GaSe (Figure 2c) [16]. An external PM angle θ_{ex} from 15° to 61° corresponds to a tuning range of 0.146–1.79 THz.

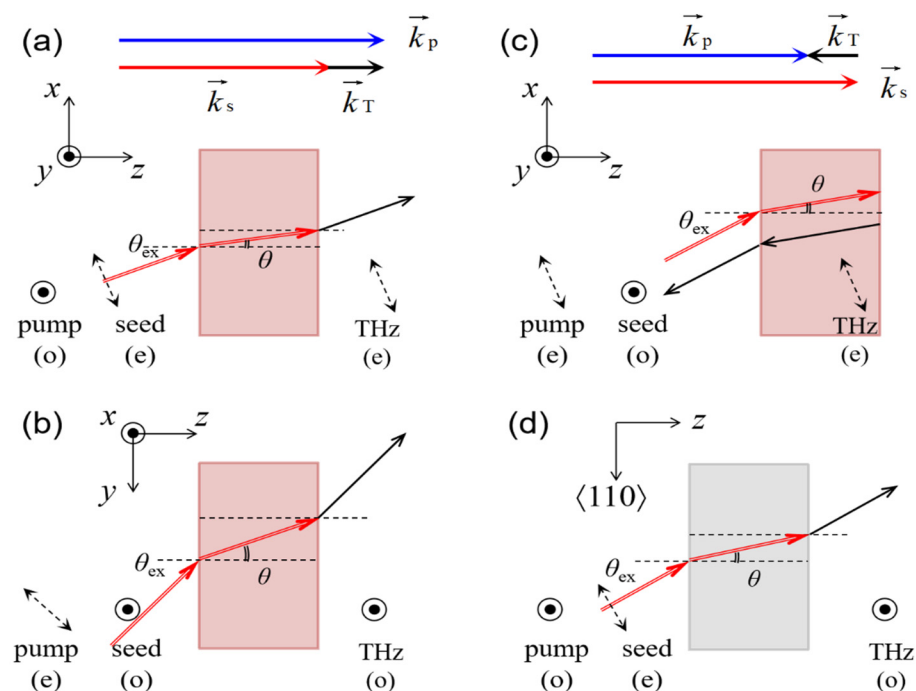


Figure 2. Schematic diagram of birefringent PM configurations: (a) oee-type, (b) eoo-type, (c) backward in GaSe, and (d) oeo-type in ZnGeP₂.

In a positive uniaxial ZnGeP₂ crystal [36], 1.06 μm pumped oee-type (similar to Figure 2a) and oeo-type (Figure 2d) PMs provide tuning ranges of 0.18–3.61 and 0.21–3.74 THz with $d_{\text{eff}} = d_{36}\sin 2\theta\cos 2\varphi$ and $d_{36}\sin\theta\sin 2\varphi$, respectively. It should be noted that the o- and e-lights in ZnGeP₂ are fast and slow lights, respectively. Moreover, birefringent PMs via other d-tensor elements such as the d_{12} of DAST [39] and the d_{15} and d_{22} of LiNbO₃ (both forward and backward) [40,41] have been reported.

Angle tuning has been used in most of the studies above. As a critical PM with small angular acceptance [34], the precise control and simultaneous adjustment of the pump wavelength and PM angle are necessary. Temperature tuning has rarely been utilized in noncritical PMs because THz absorption greatly increases with temperature [42,43]. An advantage of birefringent PMs is that there are multiple choices of pump sources. For example, GaSe-DFGs have been pumped at wavelengths of $\sim 1 \mu\text{m}$ [15,32], $\sim 1.5 \mu\text{m}$ [31], and $\sim 2 \mu\text{m}$ [34]. A drawback is the limited kinds of media. The mechanical fabrication and growth of high-quality GaSe are still difficult. Recently developed ϵ -GaSe [44] and S-doped GaSe [45] have improved the optical properties.

Cross-Reststrahlen Band Phase-Matching

This type of PM is named after the fact that THz and pump frequencies lie across the absorption band [46]. In some materials with proper phonon–polariton dispersion, the mismatch of the refractive indices can be minimized without birefringence. It has been used in isotropic zinc blende [23] and in organic crystals (also called type-0/eee-type PM) [24].

Zinc blende crystals are an excellent THz medium owing to their high nonlinearity, acceptable THz absorption, and well-developed growth and fabrication technique. This type of PM overcomes the drawback of these crystals: their intrinsic isotropy, if the pump wavelength is properly chosen. For GaP (with a transverse optical phonon frequency at 10.9 THz), the optimally matched wavelength lies at 0.9–1 μm and is delivered from an optical parametric oscillator (OPO) [23]. Commercial 1.06 μm laser-pumped GaP collinear DFG has been presented in a number of reports [47–49]. Although it is not perfectly matched, the coherence length ($l_c = \pi / |\Delta k|$) is sufficiently large, and the pump source is much more powerful. Alternative materials such as GaAs and ZnTe have transverse optical phonon frequencies at 8.1 THz and 5.32 THz and an optimally matched wavelength at $\sim 1.3 \mu\text{m}$ and $\sim 0.8 \mu\text{m}$ [50]. These crystals should be cut by $\langle 110 \rangle$ or $\langle 111 \rangle$ to utilize the element d_{14} . A comprehensive comparison between several nonlinear crystals in collinear DFG was carried out in [51].

Organic crystals with a “D- π -A” molecule/ion structure have been invented and have been applied as THz emitters [52], featuring extremely large proportions of nonlinear diagonal elements d_{11}/d_{33} and a favorable eee-type PM. A main discrepancy of these inorganic crystals is their multiple absorption peaks. In some red-colored organic crystals (DAST [24], DSTMS [53], and OH1 [54]), the matched pump wavelength lies in the range of 1.2–1.6 μm ; in yellow-colored crystals (BNA [55]), the matched pump wavelength is in the range of 0.8–0.9 μm . Apart from the OPOs [24,53–57], different kinds of lasers have been employed in this band, including Nd-doped solid-state lasers [58–60], Er-doped fiber lasers [61], and Cr:Mg₂SiO₄ lasers [62]. The high nonlinearity and THz absorption can be attributed to a short optimal interaction length (crystal thickness commonly below 1 mm [53,63]). As a result, the extremely wide tuning range (up to 30 THz) spans over the absorption bands (those of inorganic crystals are generally limited to below the transverse optical phonon frequency). Moreover, the dependence on the pump wavelength becomes insensitive [53,54], and the synchronized and precise control during frequency tuning is not necessary. The cascaded DFG process is possible when using this type of PM [63,64], which can overcome the quantum defect-related limitations of THz-DFG. An additional potential benefit of organic crystals lies in their designable molecule/ion structure, which allows us to synthesize new crystals with better optical and growing properties (e.g., the derivatives DSTMS, DASB [65], and DASC [66] as well as hydrogen-bonded MLS [67]).

Quasi-Phase-Matching (QPM)

A periodical structure with alternating sign of $\chi^{(2)}$ can extend the effective conversion length, even if the inherent coherence length is small. This configuration is called QPM and is a feasible solution to the PM problem in three kinds of media: isotropic, strongly superluminal, and those with $\Delta k > 0$. The structure can be fabricated by periodically poling a bulk crystal (ferroelectric PPLN [26,27]) or by stacking inverted layers (such as

GaP [11,68], GaAs [69,70], and OH1 [71]). The poling/inverting period Λ should be twice the coherence length, and the wavevector mismatch can be compensated for by a grating vector of $2\pi/\Lambda$ (as shown in Figure 3a).

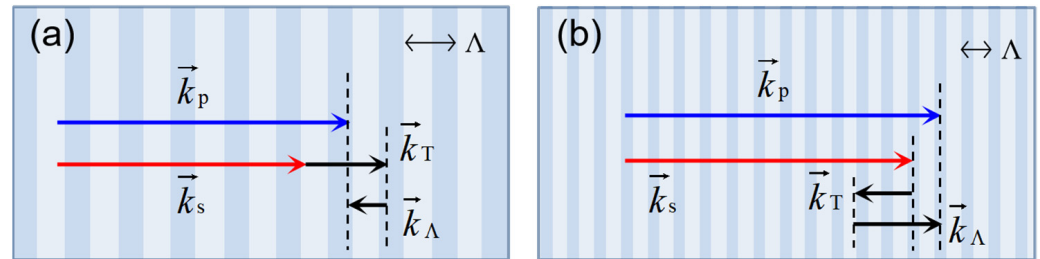


Figure 3. Orientation of wavevectors for forward (a) and backward (b) QPM.

The availability of various LiNbO₃/LiTaO₃-based periodical/apperiodical structures, including chessboard-like [72], ridged [73], slant-stripe [74], fanned-out [75], and other pre-designed structures [76,77], have the benefits of ferroelectric properties and the poling technique. The first three geometries will be discussed in Section 4. Other types of QPM crystals based on zinc blende wafers should mainly be fabricated via three methods: optical-contacted, diffusion-bonded, and orientation-patterned. A given period Λ commonly matches with one specific frequency and leads to a narrow tuning range [78]. Fanned-out structures [75] and high-order QPM [69] could widen the tuning range to some extent. Some pre-designed configurations with a gradually changing poling period could compress the phase mismatch at different cascading orders caused by crystal dispersion [77]. Continuous-wave (CW) TPO via backward QPM (as seen in Figure 3b) has been reported in PPLN [27].

The optical rectification of ultra-short laser pulses in QPM structures could also give rise to monochromatic THz-waves [78,79]. From the point of view of the time-domain, a multi-cycle wave package is generated by the inverted domains; from the point of view of the frequency-domain, one single frequency is selected by the PM condition. Another DAST-SiO₂ multi-layer structure (slightly different from QPM) has been proposed to enhance the single-cycle THz-wave output via phase correction [80].

4. Vector Phase-Matching

All of the configurations in this category utilize vector triangles and can help to solve scalar PM problems when $\Delta k < 0$. In other words, vector PM works if and only if the optical group index is smaller than the THz index. As a matter of fact, this condition is valid in a large number of materials. A variety of vector PM geometries have been invented [13,14,17,19]. We can classify them into two divisions: macroscopic noncollinear PM and microscopic vector PM. In the former case, two optical beams (commonly collimated) are obviously noncollinear and deliver a THz beam in a third direction (as seen in [17] and in the k -vector diagram in Figure 4a). In the latter case, optical beams (sometimes tightly focused) propagate in approximately the same direction, and vector PM occurs between the spatial Fourier components (such as the Cherenkov-type components [13]). Some of these methods were initially adopted for optical rectification and were later applied to dual-wavelength DFG. Here, “macroscopic” and “microscopic” are used to distinguish these divisions due to the peculiarity of THz-waves. In the traditional optical region, only the former exists, and the “vector” PM is equivalent to the “noncollinear” PM. The prominent transverse THz wavevector components contribute to the microscopic vector PM.

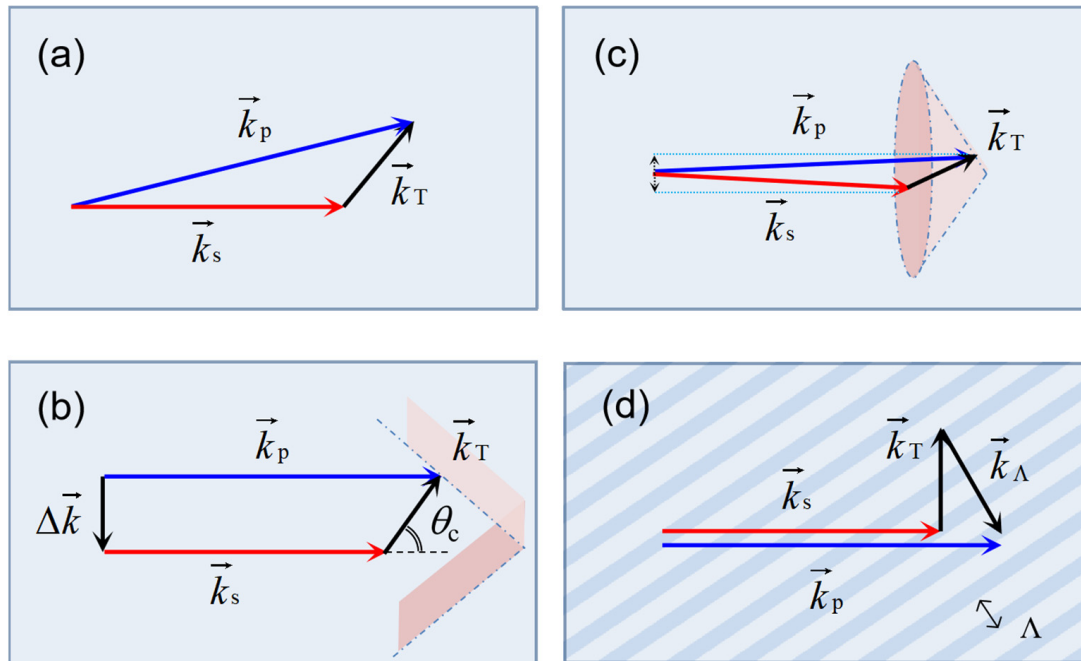


Figure 4. k -vector diagrams of different types of vector PM: (a) macroscopic noncollinear PM, (b) Cherenkov-type PM, (c) PM pumped by Bessel beam, and (d) surface-emitted QPM with slant-stripe-type poling period.

4.1. Macroscopic Noncollinear Phase-Matching

Noncollinear laser-pumped THz-wave generation began being investigated as early as 1969 [81]. This configuration is suitable for ferroelectrics, zinc blende, and KTiOPO₄ (KTP)-type media. A small angle between the two optical beams (generally below 5°) is sufficient to eliminate the wavevector mismatch, which should be synchronously changed during frequency tuning. To efficiently couple out the THz beam, traditional rectangular crystals are usually cut at an angle [82] or are attached with a Si prism [17].

As discussed above, the pump wavelength of isotropic crystals in collinear PM is determined by the dispersion property, which greatly limits the choice of pump source. This noncollinear approach makes it possible to match with a wide range of optical wavelengths. For example, 2.97 THz [82], 0.5–3 THz [83], and 0.11–4.15 THz [84] were generated using GaAs pumped by CO₂ lasers. GaP can provide a wider tuning range (up to 6 THz) due to its higher transverse optical phonon frequency. Experiments have been performed with pump sources such as Nd:YAG lasers and OPO [85], Cr:Mg₂SiO₄ lasers [86], and fiber amplifiers [87–89]. Compared to the ~0.9 μm OPO [23], some of these lasers have better performance, demonstrating higher output power and a narrower linewidth and operation at a higher repetition rate or CW. A frequency-domain THz spectrometer based on CW GaP-DFG equipped with power/frequency feedback, motorized stages, and a Si bolometer with a high spectral resolution was constructed and applied for the quality evaluation of pharmaceuticals [8].

LiNbO₃ crystals are the most studied crystal type in TPO [10,17,90–93] and is-TPG [9,94–98], as they can take advantage of the A₁-symmetry polariton mode. TPO only requires a single- and fixed-wavelength input; commercial and compact Q-switched Nd:YAG lasers are available. The THz frequency is tuned continuously by rotating the cavity of the Stokes light. Progress has been made in surface-emitted geometry via internal total reflection [10,92], pump recycling [90], and the ring cavity [91]. CW-TPO was achieved by putting a Si prism-coupled MgO:LiNbO₃ crystal within an end-pumped Nd:GdVO₄ laser resonator [93]. Later, sub-nanosecond (sub-ns) or picosecond (ps) lasers were employed as the pump source, combining a tunable seed and forming an is-TPG to pursue high peak power [94–99]. A real-time spectroscopic measurement system based on a multi-frequency

is-TPG was set up by inputting five seed beams simultaneously [9]. Noncollinear DFGs have also been conducted in bulk LiNbO₃ crystals using, for example, a CW fiber-laser pump [100] and a reflected signal beam [101].

A similar TPO configuration was also extended to Raman-active KTP-type crystals (such as KTiOPO₄ [102], KTiOAsO₄ [103], and RbTiOPO₄ [104]). The high optical damage threshold allows us to use high pump power and to obtain high nonlinear gains. Due to the infrared absorption by the A₁ crystalline modes in these crystals, discrete tuning bands were observed. A green laser pump moved the tuning bands toward higher frequencies [105].

4.2. Microscopic Vector Phase-Matching

Cherenkov-Type Phase-Matching

Classical Cherenkov radiation with a conic wavefront was first discovered in an experiment on the glow of uranyl salt solutions under gamma-ray irradiation in 1934 [106]. A similar radiation form excited by an electromagnetic pulse (called “optical Cherenkov radiation”) was predicted in 1962 [107] and was experimentally observed in optical rectification in 1984 [108]. Later, it was regarded as a kind of PM [109]. Since 2008 [13], Cherenkov-type PM in monochromatic THz-DFG has been studied. Different from the classical/optical Cherenkov radiation explained by Huygens’ principle, this Cherenkov-type PM is essentially a type of vector PM (shown in Figure 4b). It has been considered that PM is automatically satisfied under a certain angle with respect to the laser path ($\cos\theta_c = n_g/n_T$). General pump beams with a finite size consist of a continuum of radial wavenumbers that create the transverse components of Cherenkov wavevectors as long as the beam is focused into a specific size according to the THz wavelength.

This kind of PM has been demonstrated in ferroelectric LiNbO₃ [13,110–113] and in organic DAST [114] crystals. Theoretical models based on the analytical solution via spatial Fourier expansion [18] and coupled wave equations via the split-step method [115] have been reported. Line-focused pump beams can generate a wedged THz wavefront [116], which is better to collect than a conic one. Similar to in Section 4.1, Si prism coupling can decrease the absorption and increase the output, especially at high frequencies [117]. Moreover, real-time sensing with a Cherenkov-type evanescent wave has been achieved [118]. This “automatic” PM has a large tolerance (free from the precise control of input parameters) and is almost independent of the pump wavelength [119]. Strictly speaking, it is not a perfect PM type because of the transverse mismatch [110]. A small pump beam width corresponds to a wide tuning range and high efficiency. This means that a good pump beam quality is favorable. On the other hand, a narrow focus causes severe divergence, decreasing the effective radiation length. This contradiction can be solved by employing a leaky-mode waveguide, which will be discussed in the following sections.

Another PM geometry with Bessel-type pump beams was introduced [19]. By properly controlling the input beam profile (as well as the longitudinal wavenumber), oblique THz wavevectors can be generated via vector PM (as seen in Figure 4c), forming a conic wavefront. Compared to the Cherenkov-type PM above, the radial Fourier component of the Bessel pump beam is a single value that should strictly obey the PM conditions in Figure 4c. Using pump beams with a tilted phase front is an alternative approach for PM in superluminal materials [14] and is extended from optical rectification [120].

Surface-Emitted QPM with 2D Poling Period

In Section 3, collinear QPM with a longitudinal poling period was presented. A well-developed PPLN crystal has been widely used in TPO and DFG. One of the drawbacks is the high THz absorption, which limits the effective length. Surface emission achieved by tightly focusing the pump beam was proposed to minimize absorption [121,122]. The perpendicular THz wavevector originates from the transverse Fourier component (similar to Cherenkov-type PM). It still suffers from the contradiction between transverse mismatch and beam divergence. A two-dimensional (2D) poling period provided a transverse grating vector (e.g., Figure 4d), and so tight focusing was no longer necessary. Chessboard-like [72]

and ridged [73] PPLN-based DFG have been demonstrated experimentally. Another domain structure, walling along the propagation direction of optical beams, was designed, which delivered a THz beam at around the Cherenkov angle [123]. Cavity-enhanced CW THz DFG was achieved with a slant-stripe-type PPLN pumped by vertical external cavity surface-emitting lasers [74]. Similar poling structure also benefited a novel cavity-less backward TPO [124].

Modal Phase-Matching in a Waveguide

A nonlinear waveguide is a substitute for bulk crystal-based THz emitters due to modal PM and optical field confinement. By introducing the size parameter (transverse mode distribution), the THz effective index can be changed at will, to match the optical waves. As early as 1974 [12], a planar dielectric GaAs waveguide pumped by CO₂ lasers had been reported. Components made of zinc blende materials, including planar [125,126], rod [127], and ridge-type [128] components, commonly operate in guided-mode. THz output is coupled in the forward direction, and it is sometimes treated as “collinear”. However, it is intrinsically a kind of vector PM (between longitudinal propagation constants). A comprehensive comparison between different zinc blende materials for dielectric waveguide creation has been presented [129], deriving a general figure of merit for the evaluation of conversion efficiency. All-fiber CW THz generation was demonstrated experimentally based on thermal poling-induced second-order nonlinearity [130]. In these guided-mode PMs, the tuning ranges are relatively narrow, as determined by the distribution of the intrinsic mode. Another drawback lies in the coupling efficiency of the pump into the nonlinear core (small aperture), which limits the total output power.

Leaky-mode (sandwich-like) waveguides have also been applied for nonlinear THz-wave generation, which is the combination of Cherenkov-type PM and the waveguide structure [131–134]. The optical fields are confined in a high-nonlinear core (e.g., MgO:LiNbO₃) with a small cross section and deliver a leaky-mode THz-wave coupled into a Si clad. The tuning range is wider and flatter [132] due to the continuously distributed leaky mode. A room-temperature CW THz spectrometer was constructed based on this configuration, which offered broad spectral coverage (up to 7.5 THz), a high spectral resolution, a μ W-level emission power, and an absolute frequency reference [135]. Intracavity THz DFG in a dual-wavelength mid-infrared quantum cascade laser (QCL) was achieved [136]. The QCL was designed to have giant optical nonlinearity in the active region and to form a multi-layer leaky-mode waveguide, which offered efficient nonlinear conversion and output coupling.

Other Phase-Matching Configurations

There are some PM geometries that are not included in the categories above. The concept of phase correction, a situation in which the velocities of the interactive waves are not perfectly matched, was introduced in 1962 [137]. A phase shift of 180° could help to circumvent the mismatch, which is possible at the total reflection point [138] or within a Fabry–Perot interferometer (called “cavity PM”) [139,140]. Triply resonant DFG has also been analyzed theoretically [141]. The form of the resonator could be a sheet or a microdisk (in whispering gallery mode) [142]. A hybrid thin-film waveguide-based racetrack resonator was proposed recently, which gave rise to an integrated CW THz source [143].

5. Summary and Discussion

As optical THz sources (DFG, TPO, or is-TPG) mainly consist of nonlinear crystals and pump lasers, the output characteristics are greatly determined by these two factors. Different kinds of crystals have been investigated, ranging from traditional infrared (GaSe/ZnGeP₂), zinc blende (GaAs/GaP), ferroelectrics (LiNbO₃), and KTP-type (KTiOPO₄/KTiOAsO₄) crystals to organic crystals (DAST/OH1). At present, each kind has its particular advantages and inherent difficulties. An ideal nonlinear medium should exhibit the following merits: high nonlinearity, a wide transparency range, a high optical damage threshold, and fixability for large-size growth and fabrication. Since optical

THz sources are superior due to their continuous and wide tunability, the corresponding pump/seed should generally be tunable. Initially, Q-switched laser-pumped OPOs were employed, which commonly operated in ns-pulses with low repetition rates. Later, tunable lasers with amplifiers at the desired wavelength bands were developed, offering a narrower linewidth, better beam quality, acceptable power, and a high repetition rate or even CW operation.

Phase-matching represents an important connection between the two parts above. A favorable PM configuration could make full use of the merits of current lasers and crystals (some are commercially available and have demonstrated high performance) and could overcome their drawbacks. Traditional infrared crystals are suitable for birefringent PM with angle tuning. Zinc blende crystals could adopt cross-reststrahlen band PM, QPM, nonlinear PM, Bessel-type PM, guided-mode PM, and cavity PM. Ferroelectrics and KTP-type crystals could adopt QPM, nonlinear PM, Cherenkov-type PM, front-tilting PM, and leaky-mode PM. Organic crystals commonly use type-0 PM. As it is highly desired in frequency-domain THz spectroscopy, efficient nonlinear conversion under relatively low pump power is in demand. Integrated devices (e.g., fiber-coupled or on-a-chip) are arising as a new trend. A well-designed PM becomes necessary, which could relax the matching condition in a wide range of crystals and pumps and could finally promote the application of coherent THz sources.

Author Contributions: Conceptualization, P.L.; investigation, C.N. and W.L. (Wei Li); resources, W.L. (Weifan Li), Q.F. and L.G.; writing—original draft preparation, P.L. and C.N.; writing—review and editing, P.L., C.N. and Z.L.; visualization, P.L. and C.N.; supervision, F.Q.; project administration, F.Q.; funding acquisition, P.L. and F.Q. All authors have read and agreed to the published version of the manuscript.

Funding: This research was funded by the Youth Innovation Promotion Association CAS (2019204); “XingLiaoYingCai” Talents of Liaoning Province (XLYC2007074); and Young and Middle-Aged Scientific and Technological Innovation Talents of Shenyang (RC200512).

Conflicts of Interest: The authors declare no conflict of interest.

References

1. Siegel, P.H. Terahertz Technology. *IEEE Trans. Microw. Theory Tech.* **2002**, *50*, 910–928. [CrossRef]
2. Haddad, J.E.; Bousquet, B.; Canioni, L.; Mounaix, P. Review in terahertz spectral analysis. *Trends Anal. Chem.* **2013**, *44*, 98–105. [CrossRef]
3. Cehrz, R.D.; Becklin, E.E.; De Buizer, J.; Herter, T.; Keller, L.D.; Krabbe, A.; Marcum, P.M.; Roellig, T.L.; Sandell, G.H.L.; Temi, P. Status of the Stratospheric Observatory for Infrared Astronomy (SOFIA). *Adv. Space Res.* **2011**, *21*, 2551–2560.
4. Duling, I.; Zimdars, D. Terahertz imaging: Revealing hidden defects. *Nat. Photonics* **2009**, *3*, 630–632. [CrossRef]
5. Arbab, M.H.; Winebrenner, D.P.; Dickey, T.C.; Chen, A.; Klein, M.B.; Mourad, P.D. Terahertz spectroscopy for the assessment of burn injuries in vivo. *J. Biomed. Opt.* **2013**, *18*, 077004-1–077004-8. [CrossRef]
6. The Truth about Terahertz. Available online: <https://spectrum.ieee.org/aerospace/military/the-truth-about-terahertz> (accessed on 17 August 2012).
7. Sun, H.Q.; Ding, Y.J.; Zotova, I.B. THz Spectroscopy by Frequency-Tuning Monochromatic THz Source: From Single Species to Gas Mixtures. *IEEE Sens. J.* **2010**, *10*, 621–629. [CrossRef]
8. Sasaki, T.; Sakamoto, T.; Otsuka, M. Sharp Absorption Peaks in THz Spectra Valuable for Crystal Quality Evaluation of Middle Molecular Weight Pharmaceuticals. *J. Infrared Millim. Terahertz Waves* **2018**, *39*, 828–839. [CrossRef]
9. Murate, K.; Kawase, K. Perspective: Terahertz wave parametric generator and its applications. *J. Appl. Phys.* **2018**, *124*, 160901. [CrossRef]
10. Ikari, T.; Zhang, X.B.; Minamide, H.; Ito, H. THz-wave parametric oscillator with a surface-emitted configuration. *Opt. Express* **2006**, *14*, 1604–1610. [CrossRef]
11. Petersen, E.B.; Shi, W.; Chavez-Pirson, A.; Peyghambarian, N.; Cooney, A.T. Efficient parametric terahertz generation in quasi-phase-matched GaP through cavity enhanced difference-frequency generation. *Appl. Phys. Lett.* **2011**, *98*, 121119. [CrossRef]
12. Thompson, D.E.; Coleman, P.D. Step-Tunable Far Infrared Radiation by Phase Matched Mixing in Planar-Dielectric Waveguides. *IEEE Trans. Microw. Theory Tech.* **1974**, *22*, 995–1000. [CrossRef]
13. Suizu, K.; Shibuya, T.; Akiba, T.; Tutui, T.; Otani, C.; Kawase, K. Čherenkov phase-matched monochromatic THz-wave generation using difference frequency generation with a lithium niobate crystal. *Opt. Express* **2008**, *16*, 7493–7498. [CrossRef]

14. Bakunov, M.I.; Tsarev, M.V.; Mashkovich, E.A. Terahertz difference-frequency generation by tilted amplitude front excitation. *Opt. Express* **2012**, *20*, 28573–28585. [[CrossRef](#)] [[PubMed](#)]
15. Shi, W.; Ding, Y.J.; Fernelius, N.; Vodopyanov, K. Efficient, tunable, and coherent 0.18–5.27-THz source based on GaSe crystal. *Opt. Lett.* **2002**, *27*, 1454–1456. [[CrossRef](#)] [[PubMed](#)]
16. Ding, Y.J.; Shi, W. From backward THz difference-frequency generation to parametric oscillation. *IEEE J. Sel. Top. Quantum Electron.* **2006**, *12*, 352–359. [[CrossRef](#)]
17. Shikata, J.I.; Kawase, K.; Karino, K.I.; Taniuchi, T.; Ito, H. Tunable terahertz-wave parametric oscillators using LiNbO₃ and MgO:LiNbO₃ crystals. *IEEE Trans. Microw. Theory Tech.* **2000**, *48*, 653–661. [[CrossRef](#)]
18. Liu, P.X.; Xu, D.G.; Jiang, H.; Zhang, Z.; Zhong, K.; Wang, Y.Y.; Yao, J.Q. Theory of monochromatic terahertz generation via Cherenkov phase-matched difference frequency generation in LiNbO₃ crystal. *J. Opt. Soc. Am. B* **2012**, *29*, 2425–2430. [[CrossRef](#)]
19. Liu, P.X.; Shi, W.; Xu, D.G.; Zhang, X.Z.; Zhang, G.Z.; Yao, J.Q. Efficient phase-matching for difference frequency generation with pump of Bessel laser beams. *Opt. Express* **2016**, *27*, 628–630. [[CrossRef](#)]
20. Kitaeva, G.K. Terahertz generation by means of optical lasers. *Laser Phys. Lett.* **2008**, *5*, 559–576. [[CrossRef](#)]
21. Boyd, R.W. *Nonlinear Optics*, 3rd ed.; Academic Press: New York, NY, USA, 2008; pp. 77–79.
22. Powers, P.E.; Haus, J.W. *Fundamentals of Nonlinear Optics*, 2nd ed.; CRC Press: Boca Raton, FL, USA, 2019; pp. 124–125.
23. Taniuchi, T.; Nakanishi, H. Collinear phase-matched terahertz-wave generation in GaP crystal using a dual-wavelength optical parametric oscillator. *J. Appl. Phys.* **2004**, *95*, 7588–7591. [[CrossRef](#)]
24. Taniuchi, T.; Okada, S.; Nakanishi, H. Widely tunable terahertz-wave generation in an organic crystal and its spectroscopic application. *J. Appl. Phys.* **2004**, *95*, 5984–5988. [[CrossRef](#)]
25. Bakunov, M.I.; Bodrov, S.B.; Maslov, A.V.; Hangyo, M. Theory of terahertz generation in a slab of electro-optic material using an ultrashort laser pulse focused to a line. *Phys. Rev. B* **2007**, *76*, 085346. [[CrossRef](#)]
26. Wang, T.D.; Lin, S.T.; Lin, Y.Y.; Chiang, A.C.; Huang, Y.C. Forward and backward terahertz-wave difference-frequency generations from periodically poled lithium niobate. *Opt. Express* **2008**, *16*, 6471–6478. [[CrossRef](#)] [[PubMed](#)]
27. Sowade, R.; Breunig, I.; Mayorga, I.C.; Kiessling, J.; Tulea, C.; Dierolf, V.; Buse, K. Continuous-wave optical parametric terahertz source. *Opt. Express* **2009**, *17*, 22303–22310. [[CrossRef](#)] [[PubMed](#)]
28. Shi, W.; Ding, Y.J. A monochromatic and high-power terahertz source tunable in the ranges of 2.7–38.4 and 58.2–3540 μm for variety of potential applications. *Appl. Phys. Lett.* **2004**, *84*, 1635–1637. [[CrossRef](#)]
29. Tanabe, T.; Suto, K.; Nishizawa, J.; Sasaki, T. Characteristics of terahertz-wave generation from GaSe crystals. *J. Phys. D Appl. Phys.* **2004**, *37*, 155–158. [[CrossRef](#)]
30. Shi, W.; Ding, Y.J. Tunable coherent radiation from terahertz to microwave by mixing two infrared frequencies in a 47-mm-long GaSe crystal. *Int. J. High Speed Electron. Syst.* **2006**, *16*, 589–595. [[CrossRef](#)]
31. Leigh, M.A.; Shi, W.; Zhong, J.; Yao, Z.D.; Jiang, S.B.; Peyghambarian, N. Narrowband Pulsed THz Source Using Eyesafe Region Fiber Lasers and a Nonlinear Crystal. *IEEE Photonics Technol. Lett.* **2009**, *21*, 27–29. [[CrossRef](#)]
32. Zhao, P.; Ragam, S.; Ding, Y.J.; Zotova, I.B. Compact and portable terahertz source by mixing two frequencies generated simultaneously by a single solid-state laser. *Opt. Lett.* **2010**, *35*, 3979–3981. [[CrossRef](#)]
33. Huang, N.; Liu, H.J.; Sun, Q.B.; Wang, Z.L.; Li, S.P.; Han, J. Tunable terahertz generation via a cascaded optical parametric device. *Laser Phys. Lett.* **2016**, *13*, 055802. [[CrossRef](#)]
34. Yan, D.X.; Wang, Y.Y.; Xu, D.G.; Liu, P.; Yan, C.; Shi, J.; Liu, H.; He, Y.; Tang, L.; Feng, J.; et al. High-average-power, high-repetition-rate tunable terahertz difference frequency generation with GaSe crystal pumped by 2 μm dual-wavelength intracavity KTP optical parametric oscillator. *Photonics Res.* **2017**, *5*, 82–87. [[CrossRef](#)]
35. Boyd, G.D.; Bridges, T.J.; Patel, C.K.N.; Buehler, E. Phase-matched submillimeter wave generation by difference-frequency mixing in ZnGeP₂. *Appl. Phys. Lett.* **1972**, *21*, 553. [[CrossRef](#)]
36. Shi, W.; Ding, Y.J.; Schunemann, P.G. Coherent terahertz waves based on difference-frequency generation in an annealed zinc-germanium phosphide crystal: Improvements on tuning ranges and peak powers. *Opt. Commun.* **2004**, *233*, 183–189. [[CrossRef](#)]
37. Creeden, D.; McCarthy, J.C.; Ketteridge, P.A.; Schunemann, P.G.; Southward, T.; Komiak, J.J.; Chicklis, E.P. Compact, high average power, fiber-pumped terahertz source for active real-time imaging of concealed objects. *Opt. Express* **2007**, *15*, 6478–6483. [[CrossRef](#)]
38. Petersen, E.B.; Shi, W.; Nguyen, D.T.; Yao, Z.D.; Zong, J.; Chavez-Pirson, A.; Peyghambarian, N. Enhanced terahertz source based on external cavity difference-frequency generation using monolithic single-frequency pulsed fiber lasers. *Opt. Lett.* **2010**, *35*, 2170–2172. [[CrossRef](#)] [[PubMed](#)]
39. Monoszlai, B.; Vicario, C.; Jazbinsek, M.; Hauri, C.P. High-energy terahertz pulses from organic crystals: DAST and DSTMS pumped at Ti:sapphire wavelength. *Opt. Lett.* **2013**, *38*, 5106–5109. [[CrossRef](#)]
40. Akiba, T.; Seki, Y.; Odagiri, M.; Hashino, I.; Suizu, K.; Avetisyan, Y.H.; Miyamoto, K.; Omatsu, T. Terahertz wave generation using type II phase matching polarization combination via difference frequency generation with LiNbO₃. *Jpn. J. Appl. Phys.* **2015**, *54*, 062202. [[CrossRef](#)]
41. Mashkovich, E.A.; Sychugin, S.A.; Bakunov, M.I. Generation of narrowband terahertz radiation by an ultrashort laser pulse in a bulk LiNbO₃ crystal. *J. Opt. Soc. Am. B* **2017**, *34*, 1805–1810. [[CrossRef](#)]

42. Zernike, F. Temperature-Dependent Phase Matching for Far-Infrared Difference-Frequency Generation in InSb. *Phys. Rev. Lett.* **1969**, *22*, 931–933. [[CrossRef](#)]
43. Pálfalvi, L.; Hebling, J.; Kuhl, J.; Péter, Á.; Polgár, K. Temperature dependence of the absorption and refraction of Mg-doped congruent and stoichiometric LiNbO₃ in the THz range. *J. Appl. Phys.* **2005**, *97*, 123505. [[CrossRef](#)]
44. Saito, K.; Nagai, Y.; Yamamoto, K.; Maeda, K.; Tanabe, T.; Oyama, Y. Terahertz Wave Generation via Nonlinear Parametric Process from ϵ -GaSe Single Crystals Grown by Liquid Phase Solution Method. *Opt. Photonics J.* **2014**, *4*, 213–218. [[CrossRef](#)]
45. Huang, J.G.; Huang, Z.M.; Tong, J.C.; Cheng, O.Y.; Chu, J.H. Intensive terahertz emission from GaSe_{0.91}SO_{0.09} under collinear difference frequency generation. *Appl. Phys. Lett.* **2013**, *103*, 081104. [[CrossRef](#)]
46. Herman, G. Terahertz generation in high purity semiconductor via 3 wave DFG and Cross-Reststrahlen band PM. In Proceedings of the 1999 IEEE LEOS Annual Meeting Conference Proceedings, LEOS'99, 12th Annual Meeting, San Francisco, CA, USA, 8–11 November 1999.
47. Shi, W.; Ding, Y.J. Tunable terahertz waves generated by mixing two copropagating infrared beams in GaP. *Opt. Lett.* **2005**, *30*, 1030–1032. [[CrossRef](#)] [[PubMed](#)]
48. Jiang, Y.; Ding, Y.J.; Zotova, L.B. Power scaling of widely-tunable monochromatic terahertz radiation by stacking high-resistivity GaP plates. *Appl. Phys. Lett.* **2010**, *96*, 031101. [[CrossRef](#)]
49. Huang, J.G.; Lu, J.X.; Zhou, W.; Tong, J.C.; Huang, Z.M.; Chu, J.H. Investigation of high power terahertz emission in gap crystal based on collinear difference frequency generation. *Acta Phys. Sin.* **2013**, *62*, 120704. (In Chinese) [[CrossRef](#)]
50. Orlov, S.N.; Polivanov, Y.N. Spectral distribution of the efficiency of terahertz difference frequency generation upon collinear propagation of interacting waves in semiconductor crystals. *Quantum Electron.* **2007**, *37*, 36–42. [[CrossRef](#)]
51. Boulanger, B.; Bernerd, C.; Segonds, P.; Debray, J.; Roux, J.F.; Hérault, E.; Coutaz, J.L.; Shoji, I.; Minamide, H.; Ito, H.; et al. Evaluation of eight nonlinear crystals for phase-matched TeraHertz second-order difference-frequency generation at room temperature. *Opt. Mater. Express* **2020**, *10*, 561–576.
52. Jazbinsek, M.; Puc, U.; Abina, A.; Zidansek, A. Organic Crystals for THz Photonics. *Appl. Sci.* **2019**, *9*, 882. [[CrossRef](#)]
53. Liu, P.X.; Xu, D.; Li, Y.; Zhang, Y.X.; Wang, Y.Y.; Yao, J.Q.; Wu, Y.C. Widely tunable and monochromatic terahertz difference frequency generation with organic crystal DSTMS. *Europhys. Lett.* **2014**, *106*, 60001. [[CrossRef](#)]
54. Uchida, H.; Tripathi, S.R.; Suizu, K.; Shibuya, T.; Osumi, T.; Kawase, K. Widely tunable broadband terahertz radiation generation using a configurationally locked polyene 2-[3-(4-hydroxystyryl)-5,5-dimethylcyclohex-2-enylidene] malononitrile crystal via difference frequency generation. *Appl. Phys. B Lasers Opt.* **2013**, *111*, 489–493. [[CrossRef](#)]
55. Miyamoto, K.; Ohno, S.; Fujiwara, M.; Minamide, H.; Hashimoto, H.; Ito, H. Optimized terahertz-wave generation using BNA-DFG. *Opt. Express* **2009**, *17*, 14832–14838. [[CrossRef](#)] [[PubMed](#)]
56. Kawase, K.; Hatanaka, T.; Takahashi, H.; Nakamura, K.; Taniuchi, T.; Ito, H. Tunable terahertz-wave generation from DAST crystal by dual signal-wave parametric oscillation of periodically poled lithium niobate. *Opt. Lett.* **2000**, *25*, 1714–1716. [[CrossRef](#)] [[PubMed](#)]
57. Tokizane, Y.; Nawata, K.; Han, Z.L.; Koyama, M.; Notake, T.; Takida, Y.; Minamide, H. Tunable terahertz waves from 4-dimethylamino-N'-methyl-4'-stilbazolium tosylate pumped with dual-wavelength injection-seeded optical parametric generation. *Appl. Phys. Express* **2017**, *10*, 022101. [[CrossRef](#)]
58. Nawata, K.; Abe, T.; Miyake, Y.; Sato, A.; Asai, K.; Ito, H.; Minamide, H. Efficient Terahertz-Wave Generation Using a 4-Dimethylamino-N'-methyl-4'-stilbazolium Tosylate Pumped by a Dual-Wavelength Neodymium-Doped Yttrium Aluminum Garnet Laser. *Appl. Phys. Express* **2012**, *5*, 112401. [[CrossRef](#)]
59. Zhong, K.; Mei, J.L.; Wang, M.R.; Liu, P.X.; Xu, D.G.; Wang, Y.Y.; Shi, W.; Yao, J.Q.; Teng, B.; Xiao, Y. Compact High-Repetition-Rate Monochromatic Terahertz Source Based on Difference Frequency Generation from a Dual-Wavelength Nd:YAG Laser and DAST Crystal. *J. Infrared Millim. Terahertz Waves* **2017**, *38*, 87–95. [[CrossRef](#)]
60. Liu, P.X.; Qi, F.; Li, W.F.; Liu, Z.Y.; Wang, Y.L.; Ding, X.; Yao, J.Q. Self-Raman Nd-doped vanadate laser: A pump source of organic crystal based difference frequency generation. *J. Mod. Opt.* **2020**, *67*, 914–919. [[CrossRef](#)]
61. Yang, S.G.; Wang, X.J.; Wu, Z.H.; Jin, C.; Chen, M.H.; Xie, S.Z. Narrow Linewidth Terahertz Generation Engined by All-Fiber Parametric Optical Source. *IEEE Photonics J.* **2015**, *7*, 1300407. [[CrossRef](#)]
62. Vicario, C.; Jazbinsek, M.; Ovchinnikov, A.V.; Chefonov, O.V.; Ashitkov, S.I.; Agranat, M.B.; Hauri, C.P. High efficiency THz generation in DSTMS, DAST and OH1 pumped by Cr:forsterite laser. *Opt. Express* **2015**, *23*, 4573–4580. [[CrossRef](#)]
63. Liu, P.X.; Qi, F.; Pang, Z.B.; Li, W.F.; Wang, Y.L.; Liu, Z.Y.; Meng, D.L. Cascaded difference frequency generation in organic crystal 4-dimethylamino-N'-methyl-4'-stilbazolium tosylate. *Opt. Lett.* **2019**, *44*, 4965–4968. [[CrossRef](#)]
64. Liu, P.X.; Zhang, X.Y.; Yan, C.; Xu, D.G.; Li, Y.; Shi, W.; Zhang, G.C.; Zhang, X.Z.; Yao, J.Q.; Wu, Y.C. Widely tunable and monochromatic terahertz difference frequency generation with organic crystal 2-(3-(4-hydroxystyryl)-5,5-dimethylcyclohex-2-enylidene) malononitrile. *Appl. Phys. Lett.* **2016**, *108*, 011104.
65. Matsukawa, T.; Notake, T.; Nawata, K.; Inada, S.; Okada, S.; Minamide, H. Terahertz-wave generation from 4-dimethylamino-N'-methyl-4'-stilbazolium p-bromobenzenesulfonate crystal: Effect of halogen substitution in a counter benzenesulfonate of stilbazolium derivatives. *Opt. Mater.* **2014**, *36*, 1995–1999. [[CrossRef](#)]
66. Taniuchi, T.; Ikeda, S.; Mineno, Y.; Okada, S.; Nakanishi, H. Terahertz Properties of a New Organic Crystal, 4-Dimethylamino-N'-methyl-4'-stilbazolium p-Chlorobenzenesulfonate. *Jpn. J. Appl. Phys.* **2005**, *44*, L932–L934. [[CrossRef](#)]

67. Zhang, X.Y.; Jiang, X.X.; Liu, P.X.; Li, Y.; Tu, H.; Lin, Z.S.; Xu, D.G.; Zhang, G.C.; Wu, Y.C.; Yao, J.Q. Molecular design on isoxazolone-based derivatives with large second-order harmonic generation effect and terahertz wave generation. *CrystEngComm* **2016**, *18*, 3667–3673. [[CrossRef](#)]
68. Tomita, I.; Suzuki, H.; Ito, H.; Takenouchi, H.; Ajito, K.; Rungsawang, R.; Ueno, Y. Terahertz-wave generation from quasi-phase-matched GaP for 1.55 μm pumping. *Appl. Phys. Lett.* **2006**, *88*, 071118. [[CrossRef](#)]
69. Schaar, J.E.; Vodopyanov, K.L.; Kuo, P.S.; Fejer, M.M.; Yu, X.J.; Lin, A. Harris Terahertz Sources Based on Intracavity Parametric Down-Conversion in Quasi-Phase-Matched Gallium Arsenide. *IEEE J. Sel. Top. Quantum Electron.* **2008**, *14*, 354–362. [[CrossRef](#)]
70. Kiessling, J.; Breunig, I.; Schunemann, P.G.; Buse, K.; Vodopyanov, K.L. High power and spectral purity continuous-wave photonic THz source tunable from 1 to 4.5 THz for nonlinear molecular spectroscopy. *New J. Phys.* **2013**, *15*, 105014. [[CrossRef](#)]
71. Majkic, A.; Zgonik, M.; Petelin, A.; Jazbinsek, M.; Ruiz, B.; Medrano, C.; Gunter, P. Terahertz source at 9.4 THz based on a dual-wavelength infrared laser and quasi-phase matching in organic crystals OH1. *Appl. Phys. Lett.* **2014**, *105*, 141115. [[CrossRef](#)]
72. Sasaki, Y.; Avetisyan, Y.; Yokoyama, H.; Ito, H. Surface-emitted terahertz-wave difference-frequency generation in two-dimensional periodically poled lithium niobate. *Opt. Lett.* **2005**, *30*, 2927–2929. [[CrossRef](#)]
73. Suizu, K.; Suzuki, Y.; Sasaki, Y.; Ito, H.; Avetisyan, Y. Surface-emitted terahertz-wave generation by ridged periodically poled lithium niobate and enhancement by mixing of two terahertz waves. *Opt. Lett.* **2006**, *31*, 957–959. [[CrossRef](#)]
74. Paul, J.R.; Scheller, M.; Laurain, A.; Young, A.; Koch, S.W.; Moloney, J. Narrow linewidth single-frequency terahertz source based on difference frequency generation of vertical-external-cavity source-emitting lasers in an external resonance cavity. *Opt. Lett.* **2013**, *38*, 3654–3657. [[CrossRef](#)]
75. Yu, N.E.; Lee, K.-S.; Ko, D.-K.; Takekawa, S.; Kitamura, K. Fine Tuning Terahertz Generation in fanned-out periodically poled stoichiometric Lithium Tantalate Crystal. In Proceedings of the IEEE Conference on Infrared Millimeter and Terahertz Waves (IRMMW-THz), Rome, Italy, 5–10 September 2010.
76. Lee, Y.-S.; Amer, N.; Hurlbut, W.C. Terahertz pulse shaping via optical rectification in poled lithium niobate. *Appl. Phys. Lett.* **2003**, *82*, 170–172. [[CrossRef](#)]
77. Li, Z.Y.; Sun, X.Q.; Zhang, H.T.; Li, Y.J.; Yuan, B.; Jiao, B.Z.; Zhao, J.; Tan, L.; Bing, P.B.; Wang, Z.; et al. High-efficiency terahertz wave generation in aperiodically poled lithium niobate by cascaded difference frequency generation. *J. Opt. Soc. Am. B* **2020**, *37*, 2416–2422. [[CrossRef](#)]
78. Mei, J.L.; Zhong, K.; Wang, M.R.; Liu, P.X.; Xu, D.G.; Wang, Y.Y.; Shi, W.; Yao, J.Q.; Norwood, R.A.; Peyghambarian, N. Compact high-repetition-rate optical terahertz source based on difference frequency generation from an efficient 2- μm dual-wavelength KTP OPO. In Proceedings of the International Conference on Infrared, Millimeter, and Terahertz Waves (IRMMW-THz), Copenhagen, Denmark, 25–30 September 2016.
79. Vodopyanov, K.L. Optical generation of narrow-band terahertz packets in periodically-inverted electro-optic crystals: Conversion efficiency and optimal laser pulse format. *Opt. Express* **2006**, *14*, 2263–2276. [[CrossRef](#)]
80. Stepanov, A.G.; Rogov, A.; Bonacina, L.; Wolf, J.P.; Hauri, C.P. Tailoring single-cycle electromagnetic pulses in the 2-9 THz frequency range using DAST/SiO₂ multilayer structures pumped at Ti:sapphire wavelength. *Opt. Express* **2014**, *22*, 21618–21625. [[CrossRef](#)] [[PubMed](#)]
81. Yarborough, J.M.; Sussman, S.S.; Purhoff, H.E.; Pantell, R.H.; Johnson, B.C. Efficient, Tunable Optical Emission from LiNbO₃ Without a Resonator. *Appl. Phys. Lett.* **1969**, *15*, 102–105. [[CrossRef](#)]
82. Aggarwal, R.L.; Lax, B.; Favrot, G. Noncollinear phase matching in GaAs. *Appl. Phys. Lett.* **1973**, *22*, 329–330. [[CrossRef](#)]
83. Tochitsky, S.Y.; Sung, C.; Trubnick, S.E.; Joshi, C.; Vodopyanov, K.L. High-power tunable, 0.5–3 THz radiation source based on nonlinear difference frequency mixing of CO₂ laser lines. *J. Opt. Soc. Am. B* **2007**, *24*, 2509–2516. [[CrossRef](#)]
84. Lu, Y.; Wang, X.; Miao, L.; Zuo, D.; Cheng, Z. Efficient and widely step-tunable terahertz generation with a dual-wavelength CO₂ laser. *Appl. Phys. B* **2011**, *103*, 387–390. [[CrossRef](#)]
85. Tanabe, T.; Suto, K.; Nishizawa, J.; Saito, K.; Kimura, T. Tunable terahertz wave generation in the 3- to 7-THz region from GaP. *Appl. Phys. Lett.* **2003**, *83*, 237–239. [[CrossRef](#)]
86. Suto, K.; Sasaki, T.; Tanabe, T.; Saito, K.; Nishizawa, J.; Ito, M. GaP THz wave generator and THz spectrometer using Cr:Forsterite lasers. *Rev. Sci. Instrum.* **2005**, *76*, 123109. [[CrossRef](#)]
87. Nishizawa, J.; Tanabe, T.; Suto, K.; Watanabe, Y.; Sasaki, T.; Oyama, Y. Continuous-Wave Frequency-Tunable Terahertz-Wave Generation from GaP. *IEEE Photonics Technol. Lett.* **2006**, *18*, 2008–2010. [[CrossRef](#)]
88. Malinowski, A.; Lin, D.; Alam, S.U.; Zhang, Z.; Ibsen, M.; Young, J.; Wright, P.; Ozanyan, K.; Stringer, M.; Miles, R.E.; et al. Fiber MOPA based tunable source for terahertz spectroscopy. *Laser Phys. Lett.* **2012**, *9*, 350–354. [[CrossRef](#)]
89. Sasaki, T.; Tanabe, T.; Nishizawa, J. Frequency Stabilized GaP Continuous-Wave Terahertz Signal Generator for High-Resolution Spectroscopy. *Opt. Photonics J.* **2014**, *4*, 8–13. [[CrossRef](#)]
90. Wu, D.H.; Ikari, T. Enhancement of the output power of a terahertz parametric oscillator with recycled pump beam. *Appl. Phys. Lett.* **2009**, *95*, 141105. [[CrossRef](#)]
91. Minamide, H.; Ikari, T.; Ito, H. Frequency-agile terahertz-wave parametric oscillator in a ring-cavity configuration. *Rev. Sci. Instrum.* **2009**, *80*, 123104. [[CrossRef](#)]
92. Li, Z.Y.; Bing, P.B.; Yao, J.; Xu, D.; Zhong, K. High-powered tunable terahertz source based on a surface-emitted terahertz-wave parametric oscillator. *Opt. Eng.* **2012**, *51*, 091605. [[CrossRef](#)]

93. Lee, A.J.; Pask, H.M. Continuous wave, frequency-tunable terahertz laser radiation generated via stimulated polariton scattering. *Opt. Lett.* **2014**, *39*, 442–445. [[CrossRef](#)]
94. Minamide, H.; Hayashi, S.; Nawata, K.; Taira, T.; Shikata, J.; Kawase, K. Kilowatt-peak Terahertz-wave Generation and Sub-femtojoule Terahertz-wave Pulse Detection Based on Nonlinear Optical Wavelength-conversion at Room Temperature. *J. Infrared Millim. Terahertz Waves* **2014**, *35*, 25–37. [[CrossRef](#)]
95. Wu, M.-H.; Tsai, W.-C.; Chiu, Y.-C.; Huang, Y.-C. Generation of ~100 kW narrow-line far-infrared radiation from a KTP off-axis THz parametric oscillator. *Optica* **2019**, *6*, 723–730. [[CrossRef](#)]
96. Kong, W.; Li, Z.; Yan, Q.; Zou, M.; Zhou, X.; Qin, Y. Theoretical and experimental study on the enhancement of seed injection in terahertz-wave generation. *J. Opt. Soc. Am. B* **2020**, *37*, 2479–2484. [[CrossRef](#)]
97. Gao, F.; Li, Y.; Cong, Z.; Zhang, X.; Liu, Z.; Chen, X.; Qin, Z.; Wang, Z.; Ming, N. Injection-Seeded Terahertz Parametric Oscillator with a Ring-Cavity Configuration. *Crystals* **2020**, *10*, 732. [[CrossRef](#)]
98. Li, W.F.; Qi, F.; Liu, P.X.; Wang, Y.L.; Liu, Z.Y. Cascaded effect in a high-peak-power terahertz-wave parametric generator. *Opt. Lett.* **2022**, *47*, 178–181. [[CrossRef](#)]
99. Yan, C.; Xu, D.G.; Wang, Y.Y.; Wang, Z.H.; Wei, Z.Y.; Tang, L.H.; He, Y.X.; Li, J.; Zhong, K.; Shi, W.; et al. Enhanced Terahertz Wave Generation via Stokes Wave Recycling in Non-Synchronously Picosecond Pulse Pumped Terahertz Source. *IEEE Photonics J.* **2019**, *11*, 1–8. [[CrossRef](#)]
100. Wada, Y.; Satoh, T.; Higashi, Y.; Urata, Y. Compact Tunable Narrowband Terahertz-Wave Source Based on Difference Frequency Generation Pumped by Dual Fiber Lasers in MgO:LiNbO₃. *J. Infrared Millim. Terahertz Waves* **2017**, *38*, 1471–1476. [[CrossRef](#)]
101. Akiba, T.; Akimoto, Y.; Tamura, M.; Suizu, K.; Miyamoto, K.; Omatsu, T.; Takayanagi, J.; Takada, T.; Kawase, K. Broadband THz-wave generation by satisfying the noncollinear phase-matching condition with a reflected signal beam. *Appl. Opt.* **2013**, *52*, 8305–8309. [[CrossRef](#)] [[PubMed](#)]
102. Wang, W.T.; Cong, Z.H.; Chen, X.H.; Zhang, X.Y.; Qin, Z.G.; Tang, G.Q.; Li, N.; Wang, C.; Lu, Q.M. Terahertz parametric oscillator based on KTiOPO₄ crystal. *Opt. Lett.* **2014**, *39*, 3706–3709. [[CrossRef](#)]
103. Wang, W.T.; Cong, Z.H.; Liu, Z.J.; Zhang, X.Y.; Qin, Z.G.; Tang, G.Q.; Li, N.; Zhang, Y.G.; Lu, Q.M. THz-wave generation via stimulated polariton scattering in KTiOAsO₄ crystal. *Opt. Express* **2014**, *22*, 17092–17098. [[CrossRef](#)]
104. Ortega, T.A.; Pask, H.M.; Spence, D.J.; Lee, A.J. Stimulated polariton scattering in an intracavity RbTiOPO₄ crystal generating frequency-tunable THz output. *Opt. Express* **2016**, *24*, 10254–10264. [[CrossRef](#)]
105. Yan, C.; Wang, Y.Y.; Xu, D.G.; Xu, W.T.; Liu, P.X.; Yan, D.X.; Duan, P.; Zhong, K.; Shi, W.; Yao, J.Q. Green laser induced terahertz tuning range expanding in KTiOPO₄ terahertz parametric oscillator. *Appl. Phys. Lett.* **2016**, *108*, 011107. [[CrossRef](#)]
106. Cherenkov, P.A. Visible glow of pure liquids under γ -irradiation. *Dokl. Akad. Nauk. SSSR* **1934**, *2*, 451.
107. A'skaryan, G.A. Cherenkov radiation and transition radiation from electromagnetic waves. *Sov. Phys. JETP* **1962**, *37*, 594–596.
108. Auston, D.H.; Cheung, K.P.; Valdmanis, J.A.; Kleinman, D.A. Cherenkov Radiation from Femtosecond Optical Pulses in Electro-Optic Media. *Phys. Rev. Lett.* **1984**, *53*, 1555–1558. [[CrossRef](#)]
109. Hebling, J.; Almási, G.; Kozma, I.Z.; Kuhl, J. Velocity matching by pulse front tilting for large-area THz-pulse generation. *Opt. Express* **2002**, *10*, 1161–1166. [[CrossRef](#)]
110. Shibuya, T.; Tsutsui, T.; Suizu, K.; Akiba, T.; Kawase, K. Efficient Cherenkov-Type Phase-Matched Widely Tunable Terahertz-Wave Generation via an Optimized Pump Beam Shape. *Appl. Phys. Express* **2009**, *2*, 032302. [[CrossRef](#)]
111. Shibuya, T.; Suizu, K.; Kawase, K. Widely Tunable Monochromatic Cherenkov Phase-Matched Terahertz Wave Generation from Bulk Lithium Niobate. *Appl. Phys. Express* **2010**, *3*, 082201. [[CrossRef](#)]
112. Liu, P.X.; Xu, D.G.; Li, J.Q.; Yan, C.; Li, Z.X.; Wang, Y.Y.; Yao, J.Q. Monochromatic Cherenkov THz Source Pumped by a Singly Resonant Optical Parametric Oscillator. *IEEE Photonics Technol. Lett.* **2014**, *26*, 494–496. [[CrossRef](#)]
113. Akiba, T.; Akimoto, Y.; Suizu, K.; Miyamoto, K.; Omatsu, T. Evaluation of polarized terahertz waves generated by Cherenkov phase matching. *Appl. Opt.* **2014**, *53*, 1518–1522. [[CrossRef](#)]
114. Suizu, K.; Shibuya, T.; Uchida, H.; Kawase, K. Prism-coupled Cherenkov phase-matched terahertz wave generation using a DAST crystal. *Opt. Express* **2010**, *18*, 3338–3344. [[CrossRef](#)]
115. Suizu, K.; Akiba, T. Behavior of three waves in Cherenkov phase matched monochromatic terahertz wave generation investigated by numerical analysis. *Jpn. J. Appl. Phys.* **2014**, *53*, 092701. [[CrossRef](#)]
116. Stepanov, A.G.; Hebling, J.; Kuhl, J. THz generation via optical rectification with ultrashort laser pulse focused to a line. *Appl. Phys. B* **2005**, *81*, 23–26. [[CrossRef](#)]
117. Theuer, M.; Torosyan, G. Efficient generation of Cherenkov-type terahertz radiation from a lithium niobate crystal with a silicon prism output coupler. *Appl. Phys. Lett.* **2006**, *88*, 071122. [[CrossRef](#)]
118. Akiba, T.; Kaneko, N.; Suizu, K.; Miyamoto, K.; Omatsu, T. Real-time terahertz wave sensing via infrared detection interacted with evanescent terahertz waves. *Opt. Rev.* **2015**, *22*, 166–169. [[CrossRef](#)]
119. Takeya, K.; Okimura, K.; Oota, K.; Kawase, K.; Uchida, H. Pump wavelength-independent broadband terahertz generation from a nonlinear optical crystal. *Opt. Lett.* **2018**, *43*, 4100–4103. [[CrossRef](#)] [[PubMed](#)]
120. Bakunov, M.I.; Bodrov, S.B.; Tsarev, M.V. Terahertz emission from a laser pulse with tilted front: Phase-matching versus Cherenkov effect. *J. Appl. Phys.* **2008**, *104*, 073105. [[CrossRef](#)]
121. L'huillier, J.A.; Torosyan, G.; Theuer, M.; Avetisyan, Y.; Beigang, R. Generation of THz radiation using bulk, periodically and aperiodically poled lithium niobate—Part 1: Theory. *Appl. Phys. B* **2007**, *86*, 185–196. [[CrossRef](#)]

122. L’huillier, J.A.; Torosyan, G.; Theuer, M.; Rau, C.; Avetisyan, Y.; Beigang, R. Generation of THz radiation using bulk, periodically and aperiodically poled lithium niobate—Part 2: Experiments. *Appl. Phys. B* **2007**, *86*, 197–208. [[CrossRef](#)]
123. Molter, D.; Theuer, M.; Beigang, R. Nanosecond terahertz optical parametric oscillator with a novel quasi phase matching scheme in lithium niobate. *Opt. Express* **2009**, *17*, 6623–6628. [[CrossRef](#)] [[PubMed](#)]
124. Nawata, K.; Tokizane, Y.; Takida, Y.; Minamide, H. Tunable Backward Terahertz-wave Parametric Oscillation. *Sci. Rep.* **2019**, *9*, 726. [[CrossRef](#)]
125. Vodopyanov, K.L.; Avetisyan, Y.H. Optical terahertz wave generation in a planar GaAs waveguide. *Opt. Lett.* **2008**, *33*, 2314–2316. [[CrossRef](#)]
126. Saito, K.; Tanabe, T.; Oyama, Y. Widely tunable terahertz-wave generation from planar GaP waveguides via difference frequency generation under collinear phase-matching condition. *Jpn. J. Appl. Phys.* **2014**, *53*, 102203. [[CrossRef](#)]
127. Nishizawa, J.-I.; Suto, K.; Tanabe, T.; Saito, K.; Kimura, T.; Oyama, Y. THz Generation from GaP Rod-Type Waveguides. *IEEE Photonics Technol. Lett.* **2007**, *19*, 143–145. [[CrossRef](#)]
128. Saito, K.; Tanabe, T.; Oyama, Y. Polarization selective terahertz-wave generation from GaP ridge waveguide under collinear phase-matched difference-frequency mixing. *Jpn. J. Appl. Phys.* **2014**, *53*, 102102. [[CrossRef](#)]
129. Cherchi, M.; Taormina, A.; Busacca, A.C.; Oliveri, R.L.; Bivona, S.; Cino, A.C.; Stivala, S.; Sanseverino, S.R.; Leone, C. Exploiting the Optical Quadratic Nonlinearity of Zinc-Blende Semiconductors for Guided-Wave Terahertz Generation: A Material Comparison. *IEEE J. Quantum Electron.* **2010**, *46*, 368–376. [[CrossRef](#)]
130. Liu, W.L.; Zhang, J.J.; Rioux, M.; Viens, J.; Messaddeq, Y.; Yao, J.P. Frequency Tunable Continuous THz Wave Generation in a Periodically Poled Fiber. *IEEE Trans. Terahertz Sci. Technol.* **2015**, *5*, 470–477. [[CrossRef](#)]
131. Bodrov, S.B.; Bakunov, M.I.; Hangyo, M. Efficient Cherenkov emission of broadband terahertz radiation from an ultrashort laser pulse in a sandwich structure with nonlinear core. *J. Appl. Phys.* **2008**, *104*, 093105. [[CrossRef](#)]
132. Suizu, K.; Koketsu, K.; Shibuya, T.; Tsutsui, T.; Akiba, T.; Kawase, K. Extremely frequency-widened terahertz wave generation using Cherenkov-type radiation. *Opt. Express* **2009**, *17*, 6676–6681. [[CrossRef](#)]
133. Liu, P.X.; Xu, D.G.; Wang, W.P.; Liu, C.M.; Yin, S.J.; Ding, X.; Wang, Y.Y.; Yao, J.Q. Widely Tunable, Monochromatic THz Generation via Cherenkov-Type Difference Frequency Generation in an Asymmetric Waveguide. *IEEE J. Quantum Electron.* **2013**, *49*, 179–185. [[CrossRef](#)]
134. Bodrov, S.B.; Ilyakov, I.E.; Shishkin, B.V.; Bakunov, M.I. Highly efficient Cherenkov-type terahertz generation by 2- μm wavelength ultrashort laser pulses in a prism-coupled LiNbO₃ layer. *Opt. Express* **2019**, *27*, 36059–36065. [[CrossRef](#)]
135. De Regis, M.; Bartalini, S.; Ravaro, M.; Calonico, D.; De Natale, P.; Consolino, L. Room-Temperature Continuous-Wave Frequency-Referenced Spectrometer up to 7.5 THz. *Phys. Rev. Appl.* **2018**, *10*, 064041. [[CrossRef](#)]
136. Vijayraghavan, K.; Jiang, Y.; Jang, M.; Jiang, A.; Choutagunta, K.; Vizbaras, A.; Demmerle, F.; Boehm, G.; Amann, M.C.; Belkin, M.A. Broadly tunable terahertz generation in mid-infrared quantum cascade lasers. *Nat. Commun.* **2013**, *4*, 2021. [[CrossRef](#)]
137. Armstrong, J.A.; Bloembergen, N.; Ducuing, J.; Pershan, P.S. Interactions between Light Waves in a Nonlinear Dielectric. *Phys. Rev.* **1962**, *127*, 449–470. [[CrossRef](#)]
138. Raybaut, M.; Godard, A.; Lubin, C.; Lefebvre, M.; Rosencher, E. A Guided Wave Approach to Fresnel Phase Matching: Application to Parametric Oscillation and Terahertz-Wave Generation. In Proceedings of the IEEE Conference on Lasers and Electro-Optics/Quantum Electronics and Laser Science Conference and Photonic Applications Systems Technologies, Technical Digest, Long Beach, CA, USA, 21–24 May 2006.
139. Saito, K.; Tanabe, T.; Oyama, Y. Cascaded terahertz-wave generation efficiency in excess of the Manley–Rowe limit using a cavity phase-matched optical parametric oscillator. *J. Opt. Soc. Am. B* **2015**, *32*, 617–621. [[CrossRef](#)]
140. Liu, P.X.; Qi, F.; Li, W.F.; Wang, Y.L.; Liu, Z.Y.; Wu, H.M.; Ning, W.; Shi, W.; Yao, J.Q. Low-threshold terahertz-wave generation based on a cavity phase-matched parametric process in a Fabry–Perot microresonator. *J. Opt. Soc. Am. B* **2018**, *35*, 68–72. [[CrossRef](#)]
141. Burgess, I.B.; Rodriguez, A.W.; McCutcheon, M.W.; Bravo-Abad, J.; Zhang, Y.N.; Johnson, S.G.; Lončar, M. Difference-frequency generation with quantum limited efficiency in triply-resonant nonlinear cavities. *Opt. Express* **2009**, *17*, 9241–9251. [[CrossRef](#)]
142. Sinha, R.; Karabiyik, M.; Ahmadivand, A.; Al-Amin, C.; Vabbina, P.K.; Shur, M.; Pala, N. Tunable, Room Temperature CMOS-Compatible THz Emitters Based on Nonlinear Mixing in Microdisk Resonators. *J. Infrared Millim. Terahertz Waves* **2016**, *37*, 230–242. [[CrossRef](#)]
143. Yang, J.W.; Wang, C. Efficient terahertz generation scheme in a thin-film lithium niobate-silicon hybrid platform. *Opt. Express* **2021**, *29*, 16477–16486. [[CrossRef](#)]